JOURNAL OF Materials CHEMISTRY

TEM, EELS and EFTEM characterization of nickel nanoparticles encapsulated in carbon

Teresa C. Rojas,[a] María J. Sayagués,[a] Alfonso Caballero,[a] Yuri Koltypin,[b] Aharon Gedanken,[b] Laurence Ponsonnet,[c] Beatrice Vacher,[c] Jean M. Martin[c] and Asunción Fernández[a]

[a]*Instituto de Ciencia de Materiales de Sevilla and Dpto. de Química Inorgánica, Centro de Investigaciones Científicas Isla de la Cartuja, Avda, Américo Vespucio s/n, 41092 Sevilla, Spain. E-mail: asuncion@cica.es*
[b]*Departments of Chemistry and of Physics, Bar-Ilan University, Ramat-Gan, 52900, Israel*
[c]*Ecole Centrale de Lyon, Laboratoire de Tribologie et Dynamique des Systèmes, UMR 5513 ECL/CNRS, B.P.163, 69131 Ecully Cedex, France*

Received 11th October 1999, Accepted 22nd December 1999

Nickel particles dispersed in an amorphous carbon matrix have been synthesized by a sonication method, and further heated at 773 K under Ar atmosphere. Both as-prepared and heated samples have been fully characterised using different techniques such as transmission electron microscopy (TEM), high resolution TEM (HRTEM), energy dispersive X-ray analysis (EDX), X-ray absorption spectroscopy (XAS), electron energy loss spectroscopy (EELS) and energy filtered TEM (EFTEM). The as-prepared sample shows amorphous spherical particles formed by Ni^{2+} dispersed in a carbon matrix. After heating, the formation of small metallic nickel nanocrystallites inside these spherical particles is observed. The EELS spectra show a decreased oxygen content in the heated sample due to the reduction of Ni^{2+} in the presence of carbon. This result is also confirmed by XAS. In addition, the EELS and EFTEM analyses indicate that the nickel nanocrystallites are surrounded by amorphous carbon which provides some protection to the metallic nickel from oxidation.

Introduction

Research in nanostructured materials has been very active in the last decade owing to their particular properties, which are different from the conventional macroscopic materials.[1–4]

Metal nanoparticles have potential applications in many areas, especially for magnetic materials.[5–7] The unusual magnetic behaviour of these systems has been found to be dependent on the size of the particles as well as their crystallinity.

Previous work[8] has shown that carbon encapsulated nanoparticles of ferromagnetic materials are predominantly monodomain and manifest the full range of fine-particle magnetic phenomena. The interesting magnetic behaviour and oxidation resistance of carbon coated particles have led to considerations of these particles for applications in areas such as magnetic data storage, magnetic toners for xerography, ferrofluids, *etc.*

We have recently published a paper[9] concerning the preparation and the physical properties of amorphous and crystalline nickel nanoparticles encapsulated in carbon. The synthesis of the amorphous material was carried out using the ultrasonic radiation method during which a precursor decomposes under irradiation.[10] We proposed in previous work,[9] the use of $Ni(COD)_2$ (COD = cycloocta-1,5-diene) as a suitable organic precursor for the nickel synthesis. This is a more safe compound than the previously proposed nickel carbonyl.[11] However, to our knowledge, there has not been a previous full characterization at the microstructural level of such materials either in their as-prepared amorphous state or after heating treatments. Such characterization is vital for the full understanding of the magnetic properties of the samples. In particular, heated samples have shown superparamagnetic behaviour.[9]

Here, we show the application of different techniques such as TEM (transmission electron microscopy), HRTEM (high resolution TEM), EDX (energy dispersive X-ray analysis), EELS (electron energy loss spectroscopy), EFTEM (energy filtered TEM) and XAS (X-ray absorption spectroscopy) for the microstructural and chemical characterization of nickel nanoparticles encapsulated in carbon.

Experimental

Nickel nanoparticles encapsulated in carbon were obtained by a sonication method. A 0.02 M solution of $Ni(COD)_2$ in toluene was sonicated for 5 h under an Ar pressure of 1.5 atm.[9] The obtained powder (as-prepared sample) was also heated at 773 K for 20 h under a flow of pure Ar (heated sample).

The microstructural characterization and the microanalysis were performed using a variety of microscopes and associated techniques that are described below. The TEM samples were dispersed in ethanol by ultrasound and dropped on a copper grid coated with a carbon film.

(1) PHILIPS CM200 (Instituto de Ciencia de Materiales de Sevilla C.S.I.C.) with a supertwin objective lens, working at 200 kV with a LaB_6 filament and $\pm 45^\circ$ tilt side-entry specimen holder (point resolution = 0.24 nm). The instrument is equipped with a heating holder, an EDX detector (EDAX) and a PEELS spectrometer (GATAN 766-2K).

(2) JEOL 4000 EX(II) (Department of Materials, Oxford University) operating at 400 kV with a LaB_6 filament and top-entry goniometer ($\pm 20^\circ$ tilt). The point resolution is *ca.* 0.16 nm.

(3) JEOL 2010 FEG (Ecole Central de Lyon) operating at 200 kV, probed size between 0.5 and 2.4 nm, point resolution

ca. 0.19 nm. The instrument is equipped with an EDX detector (Oxford Link) and a PEELS spectrometer (GATAN 766-2K).

(4) ZEIS CEM 902 (Ecole Central de Lyon) equipped with a Castaing–Henry magnetic-sector/electrostatic-mirror and a Kontron image analysis system to produce energy-filtered images.

In order to record the EELS spectra at the C-K, O-K and Ni-$L_{2,3}$ edges the illuminated area was *ca.* 100–150 nm in diameter. Spectra were recorded in the diffraction mode with a camera length of 340 mm, a 2 mm spectrometer entrance aperture and a collection angle of *ca.* 2.03 mrad. The measured energy resolution at the zero-loss peak of the coupled microscope/spectrometer system was *ca.* 1.4 eV. To carry out quantitative analysis, a larger dispersion (eV channel^{-1}) was used in order to record C-K, O-K and Ni-$L_{2,3}$ edges simultaneously. A camera length of 340 mm and a 5 mm spectrometer aperture were used giving rise to a collection angle of 5.08 mrad and a resolution of 2.5 eV. Spectra were corrected for dark current and channel-to-channel gain variation. A low-loss spectrum was also recorded with each edge in the same illuminated area and using the same experimental conditions. After the subtraction of the background with a standard power-law function, the spectra were deconvoluted for plural scattering with the Fourier-ratio method. All these treatments were performed within the EL/P program (Gatan).

In order to collect energy-filtered images, and to obtain elemental mapping and EELS spectra from small areas a method called "Imaging-Spectrum"[12] was used. Using commercially available hardware and some specific software this method can be adapted to all energy-filtered microscopes. In this work we used the Zeis CEM 902 instrument where this method has been implemented previously. A Hewlett-Packard workstation was used for the data processing. By the "imaging-spectrum" method a series of images (256×256 pixels) are recorded with a given energy step between each image. Once the series was recorded, it is possible to select an area of interest or a single pixel, the computation process reads the grey level for each selected pixel of each image and plots a curve, energy loss *vs.* grey level, resulting in the corresponding EELS spectrum of the selected area. It is necessary to perform some major corrections in the recorded images: *viz.* second order aberrations, signal dispersion in the camera and drift of the specimen over long acquisition times. For the elemental calculations the "imaging-spectrum" method offers great potential for the choice of the images and the background calculation method.[13]

XAS spectra were recorded at the beam line BM29 in the ESRF storage ring in Grenoble running at 6 GeV, with an average current of 165 mA. Monochromatisation of the beam was carried out using an Si(111) double crystal monochromator. The detection of the XAS absorption coefficient was in the transmission mode for pressed pellets of the samples diluted in boron nitride. Spectra were recorded at the Ni K-edge at *ca.* 8330 eV. To compare the XANES (X-ray absorption near edge structure) region of the XAS spectra, a linear background was fitted in the pre-edge region and subtracted before normalisation to the edge jump. The EXAFS (extended X-ray absorption fine structure) oscillations were analysed with the software package developed by Bonin *et al.*[14] The coordination numbers (N), distances (R) and Debye–Waller factors (σ) were extracted by a least-squares fitting procedure that uses the theoretical phases and amplitudes proposed by Rehr and coworkers[15] previously calibrated with the appropriate reference (Ni foil).

Results and discussion

The as-prepared sample was studied by TEM and a micrograph at low magnification is shown in Fig. 1(a). From this, spherical amorphous particles of *ca.* 100–150 nm are clearly evident. The composition of the particles was determined by EDX analysis showing the presence of carbon and nickel. EDX spectra were taken in different areas inside different spherical particles. Examples of the spectra registered in the core and at the edge in one spherical particle are shown in Fig. 1(b) and (c) respectively. The intensity ratio between the C and Ni peaks indicates that the core is richer in Ni than the edge. As we do not observe distinguishable particles in the TEM images, the nickel phase appears to be highly dispersed in the carbon matrix.

A TEM study of the heated sample (773 K) shows, however, the formation of small nanocrystallites inside the spherical particles, as can be seen in the corresponding micrograph [Fig. 2(a)]. While some spherical particles show an average size for the nanocrystals of 2–5 nm (particles A), others showed a size of 10–20 nm (particles B) for these nanocrystals. The selected area electron diffraction pattern corresponding to this sample is shown in Fig. 2(b). The diffracted rings can be indexed to metallic cubic nickel with no evidence of nickel oxide or carbide crystal formation. This result is in good agreement with that obtained by XPS in previous work[9] and seems to indicate that the small nanoparticles embedded in the amorphous matrix are metallic nickel.

An *in situ* experiment within the TEM microscope to follow the heating transformation steps was carried out using the heating holder device (up to 873 K). Fig. 3(a)–(c) show low magnification micrographs for the as-prepared sample (a) and after heating in the microscope, at 773 K (b) and 873 K (c). From Fig. 3(a) to (c) progressive formation of small black dots is observed, which corresponds to crystallization of Ni nanoparticles (checked with the ED technique). In the majority of the particles the crystallization process started in the cores of the amorphous spherical particles where the Ni particles were found to be larger. Growth of the nickel crystals has been found to be promoted by electron-beam irradiation.

In order to obtain more information about the nickel particles, in both the as-prepared and the heated samples, X-ray absorption spectra at the Ni K-edge were recorded. By this technique chemical information, as well as structural data relating to the short range order of nanocrystalline and amorphous materials can be obtained.

Fig. 4 shows the XANES region of the XAS spectra for both samples (as-prepared and heated) and for a metallic nickel foil included as a reference. Although multiple scattering calculations can be carried out to simulate the XANES spectra, a finger print technique can also be used to obtain conclusions from these data simply by comparison with reference samples.[16] The first region in the spectra corresponds to a low energy shoulder before the edge threshold at *ca.* 8334 eV. This shoulder is usually attributed to the 1s$\rightarrow$3d transition which in perfect O_h symmetry is strictly dipole-forbidden. However, owing to the mixing of p- and d-like states this feature is visible here. The intensity of this peak is strongly dependent on the oxidation state and local structure of the nickel atoms, as demonstrated in Fig. 4. The second region of the spectra corresponds to the sharp rise for the excitation of the 1s electron into the ionization continuum. In the third region, a few eV above the threshold (8349 eV), the final states of the photoelectron should be described in terms of unoccupied bands close to the Fermi level. The intensity of this feature (white line) is also strongly dependent from the oxidation state of nickel,[16] being very intense for oxidised nickel atoms.

By comparison of the Ni-K edge XANES spectra for the as-prepared and heated samples in Fig. 4, we observe a higher intensity of the feature at 8334 eV and a lower intensity of the feature at 8349 eV for the heated sample as compared to the as-prepared sample. In this sense the heated sample is more similar to the Ni foil reference. The as-prepared sample appears to

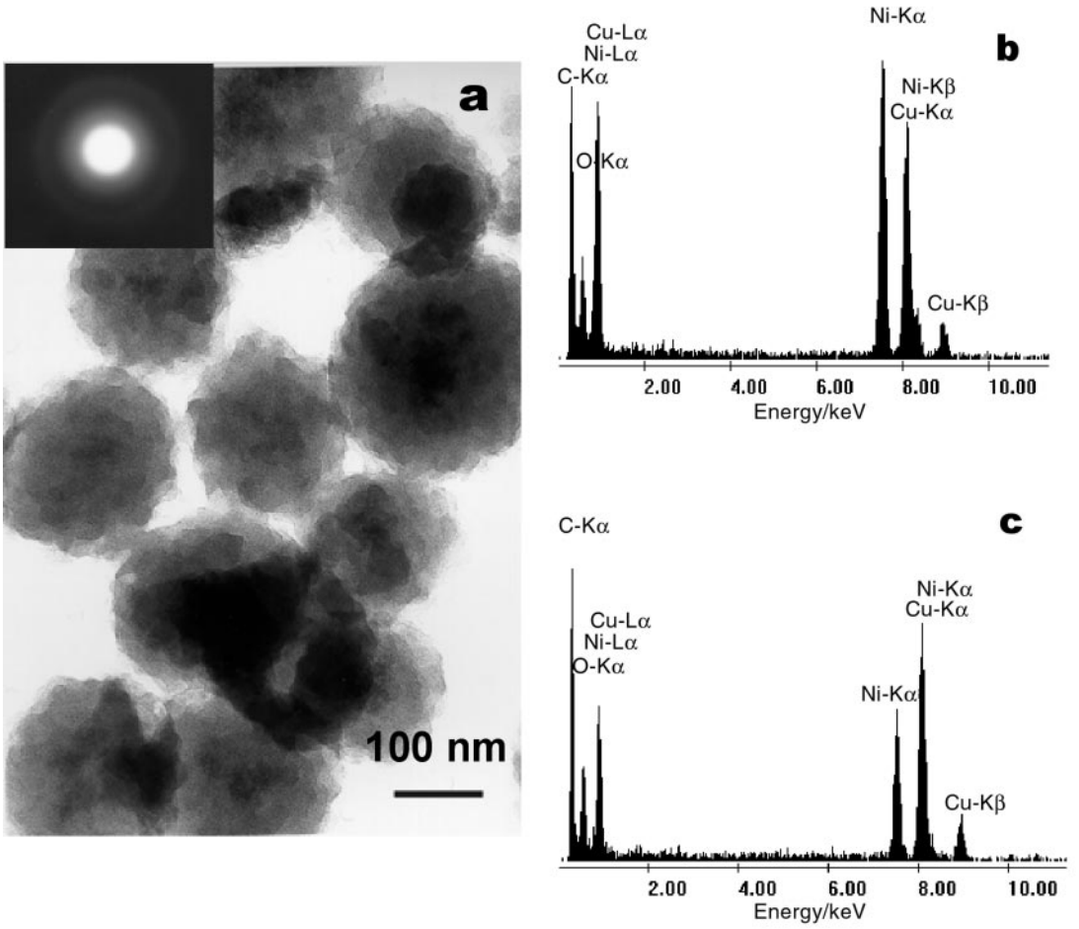

Fig. 1 (a) TEM image of the as-prepared sample and the corresponding SAED pattern; (b) and (c) EDX spectra registered at the centre and at the edge of a spherical particle, respectively.

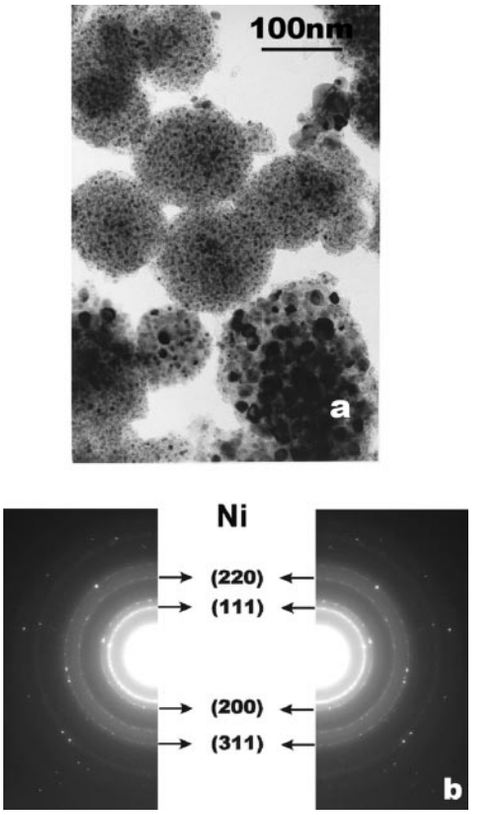

Fig. 2 (a) TEM image of the heated sample (773 K) and (b) SAED pattern from a spherical particle. All the diffraction rings correspond to metallic nickel.

contain nickel in an oxidised state that is well dispersed in the carbon matrix, as can be deduced from the TEM/EDX analysis previously described. The heating treatment leads to the partial reduction of Ni^{2+} species in the presence of carbon, as evident from the decrease in the white line intensity of this sample. This reduction may lead to the formation of the metallic nickel nanocrystalline particles detected by TEM.

The Fourier transforms of the EXAFS oscillations are shown in Fig. 5. Although a fitting procedure is needed to determine the exact position of the maxima, some conclusions can already be obtained by glancing at this Figure. The heated sample shows similar information about the coordination spheres to that observed in the nickel foil reference, the peaks being nearly coincident, although the intensities are smaller. This indicates the formation of very small nickel nanocrystallites so that a perfect long range structure could not be obtained. The information from the as-prepared sample is clearly different in terms of the coordination spheres, which is clearly visible in the first two peaks.

The fitting analysis of the EXAFS oscillations leads to the curves shown in Fig. 6(a) while quantitative results of this analysis for the first coordination spheres are summarized in Table 1. The Fourier transform curves shown in Fig. 6(b) are not corrected for any phase shift. The first peak appears, according to Table 1, at *ca.* 2.05 Å and corresponds to Ni–O distances typical of oxidised nickel. Another peak corresponding to Ni–Ni distances at 3.02–3.05 Å has been ascribed to the second coordination sphere around nickel in nickel oxide [see Fig. 6(b)]. These two peaks are present in the Ni/C as-prepared sample and diminish strongly with intensity for the heated sample as expected upon reduction of the oxidised nickel to the metal. In addition, the heated sample shows a strong peak in

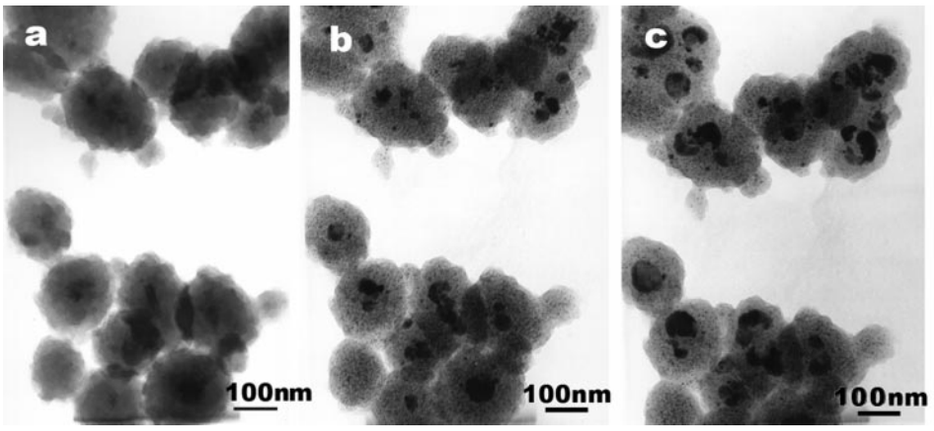

Fig. 3 TEM image evolution during the *in situ* heating experiment; (a) as prepared sample, (b) 773 K and (c) 873 K.

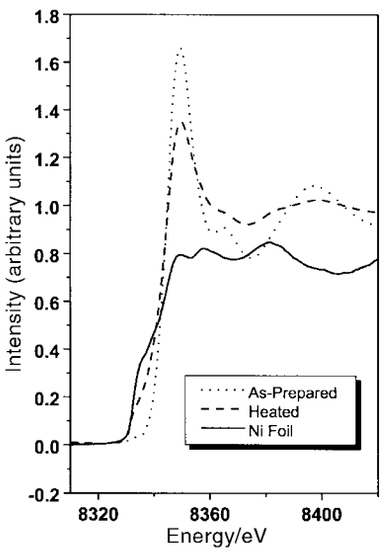

Fig. 4 XANES region at the Ni-K edge for the as-prepared and heated samples (773 K) and for a metallic nickel foil as a reference.

the Fourier transform curve at 2.48 Å that corresponds to Ni–Ni distances for metallic nickel. Additionally, Ni–C distances may be also present in the first peak at *ca.* 2.05 Å.

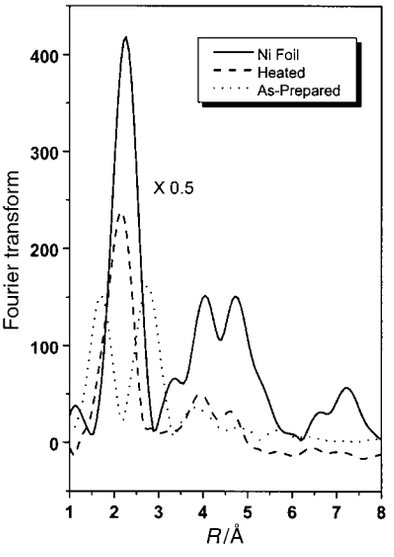

Fig. 5 Fourier transform of the EXAFS oscillations at the Ni-K edge for the as-prepared and heated samples (773 K) and for the metallic nickel foil.

Fig. 7 shows a high resolution TEM micrograph of the heated sample showing small metallic nickel crystallites embedded in the carbon matrix. Clear lattice images are observed for only the particles in which the arrangement of atom planes is parallel with the direction of the electron beam. A lattice distance is indexed in a nickel nanoparticle along the [111] zone axis.

The EELS technique in transmission electron microscopy is very appropriate for the characterization of nanostructured samples by recording core level absorption edges in an analogous way to XAS but providing information at a microscopic level.[17]

In the present work, the C-K, O-K and Ni-$L_{2,3}$ edges have been recorded in different areas for the two samples. At the microscopic level, the samples are heterogeneous showing zones with different atomic ratios of the elements. Representative results from the quantitative analysis performed in both samples are shown in Table 2. As can be seen, two different type of particles (A and B) were found in terms of Ni composition. These two types of particles correspond to the smaller and larger crystallites of the nickel phase in the heated sample, as previously found by TEM observations.

Fig. 8 shows the O-K and Ni-$L_{2,3}$ edge EELS spectra for both the as-prepared and the heated sample taken in an area of small particles and recorded after exposure to air. The spectra are normalized to the jump at the Ni-$L_{2,3}$ edge. The heated sample contains a lower amount of oxygen as is evident from the lower intensity of the O-K peak caused by the reduction of Ni^{2+} in the presence of carbon when the as-prepared sample was heated. This result was found for both particles of type A and B, as can be seen from the quantitative analysis (Table 2). Some of the detected oxygen by EELS may correspond to absorbed oxygen at the surface and in pores of the carbon matrix.

The existence of Ni^{2+} in the as-prepared sample and the reduction to metallic nickel in heated samples has already been demonstrated by XAS in the present work. In addition, these results were confirmed by the XPS results reported in previous work.[9] On the other hand, the presence of some oxidised nickel in the heated sample, as evidenced by XAS, may be due to surface oxidation of nanoparticles not fully protected by the carbon matrix.

With the purpose of analysing the composition of the areas around and within the small Ni nanoparticles, an FEG-TEM microscope was used (with a probe size of <1 nm). Fig. 9 shows a high magnification micrograph corresponding to the heated sample in an area of a spherical particle. The EELS spectra at the C K edge and Ni $L_{2,3}$-edges were recorded both outside (Fig. 9 left) and inside (Fig. 9 right) a small Ni particle. The results indicate that nickel atoms form the nanocrystallites.

In order to visualize the Ni distribution in the carbon matrix,

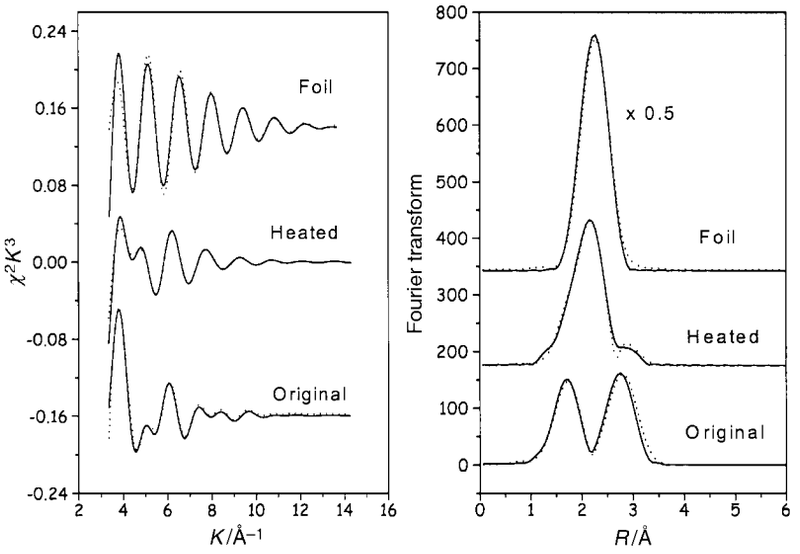

Fig. 6 EXAFS oscillations (left) and Fourier transforms (right) (not corrected for the phase shift) of the two first coordination spheres for the as-prepared and heated samples (773 K) and for a metallic nickel foil as reference. Experimental data (full line) and the fitted curves (dotted line) are shown.

Table 1 Best fitting parameters of the Ni-K edge EXAFS oscillations for the as-prepared and heated samples and for the Ni foil reference sample

Sample		N^b	R^c/Å	$10^3\Delta\sigma^{2\,d}$
Ni foil	$(Ni–Ni)_m{}^a$	11.1	2.48	
Ni/C-as-prepared	(Ni–O)	6.3	2.05	+0.68
	$(Ni–Ni)_o{}^a$	11.10	3.05	+7.50
Ni/C-heated (773 K)	(Ni–O)	2.9	2.06	−0.33
	$(Ni–Ni)_m$	2.9	2.48	−0.96
	$(Ni–Ni)_o$	7.6	3.02	+13.8

[a]$(Ni–Ni)_m$: Ni–Ni first coordination sphere for metallic nickel, $(Ni–Ni)_o$: Ni–Ni second coordination sphere for nickel oxide. [b]Coordination number. [c]Bond lengths. [d]Debye–Waller factors.

elemental mapping was performed using the "Imaged-Spectrum" method implanted in a EFTEM (Zeis CEM 902) microscope and elemental maps of carbon and nickel were calculated from the filtered images, obtained at the C-K and Ni-$L_{2,3}$ edges, respectively. To obtain the mapping and EELS

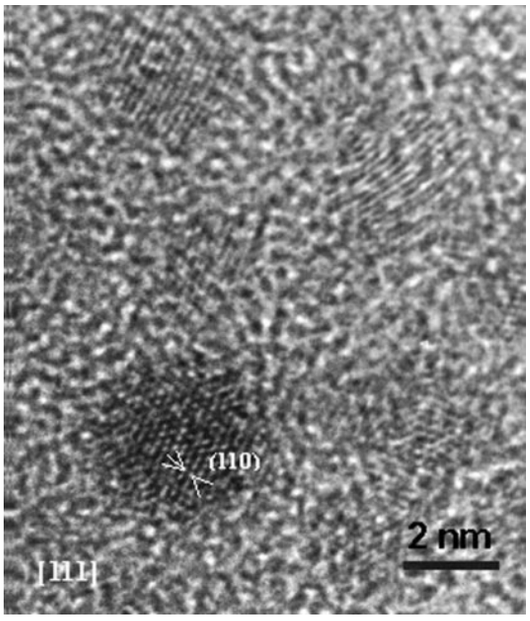

Fig. 7 HRTEM micrograph for the heated sample (773 K) showing small nickel nanoparticles.

Table 2 Quantitative results (C/O and C/Ni atomic ratios) found by the EELS technique for the original and the heated samples for two representative particles A and B

	Particle A		Particle B	
	C/O	C/Ni	C/O	C/Ni
As-prepared	4.8	12.5	4	5
Heated	15.3	8.8	11.8	4

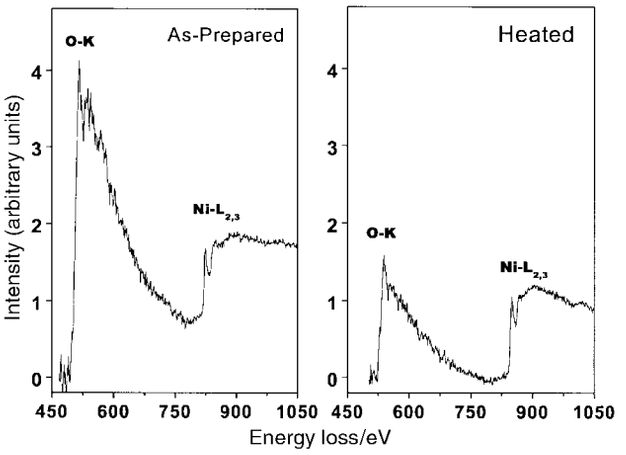

Fig. 8 EELS spectra corresponding to the as-prepared and heated samples (773 K); O-K and Ni-$L_{2,3}$ edges are shown. The edges are normalized to the Ni-$L_{2,3}$ jump.

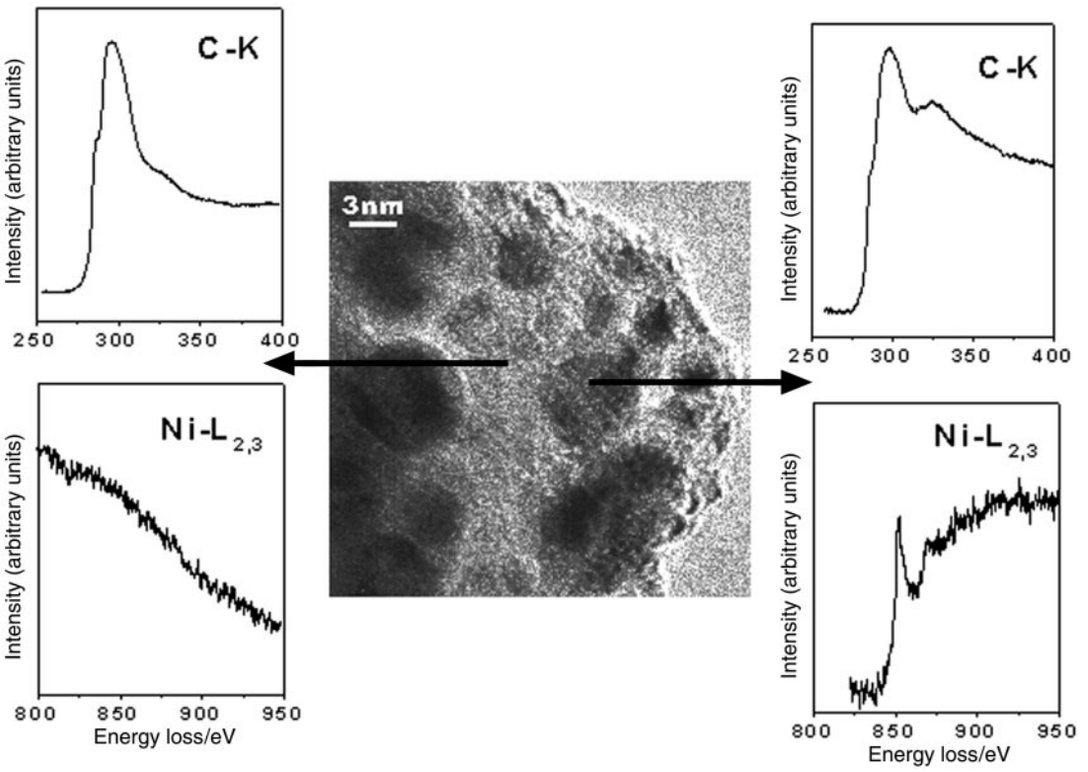

Fig. 9 TEM image of the heated sample (773 K), taken in a FEG microscope. C-K and Ni-$L_{2,3}$ edge spectra inside (right) and outside (left) of a Ni nanoparticle are shown.

spectra from different small areas, a series of 100 filtered images were recorded with an energy step of 1 eV, from 250 to 350 eV for the carbon map and from 825 to 925 eV for the nickel map. The power-law subtraction method was used to remove the background.

The composition map obtained by overlapping the C and Ni maps is shown in Fig. 10. The green and the red areas represent the carbon and nickel distributions, respectively. The EELS spectra obtained from the small square marked areas are also shown in Fig. 10. Two marked areas have been chosen with different degrees of green and red, in good agreement with the intensity of the C and Ni edges found in the calculated EELS spectra from both areas. The most reddish area contains a large quantity of Ni in the spectrum and a little carbon; although no green colour is visible carbon appears to always surround the Ni particles. The studied area with some green, red and yellow regions exhibits spectra indicating more carbon than nickel; the yellow colour may be due to a homogeneous mixture of both elements.

Finally it should be mentioned that it is possible that small quantities of C atoms are sited in the Ni lattice occupying interstitial positions. However, it is not clear from the characterization techniques used here whether such point defects are present.

Conclusions

The preparation method used in this work gives rise to a nickel nanocrystalline material which is embedded in a porous amorphous carbon layer, which leads to some protection from atmospheric oxidation.

A combination of complementary techniques has been

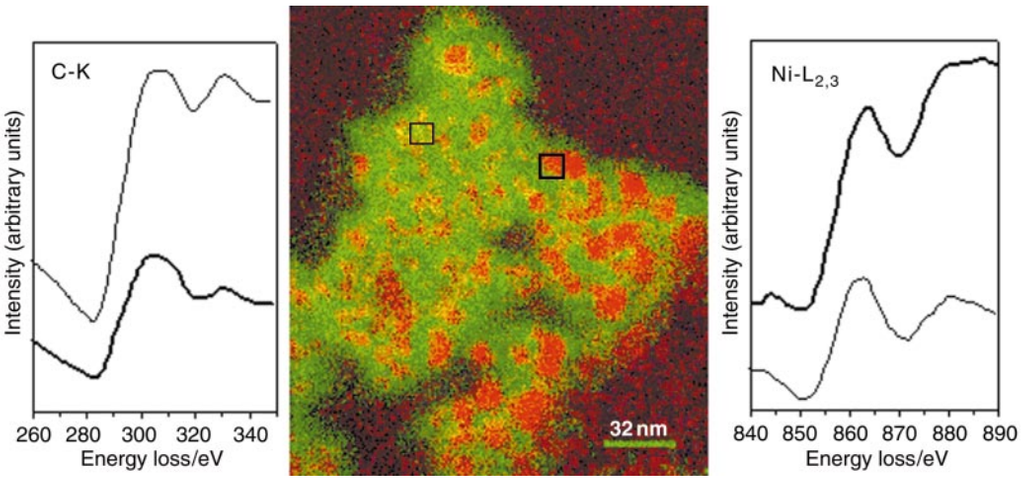

Fig. 10 Chemical map from the heated sample (773 K) (red corresponds to the Ni distribution and green to the C distribution). EELS spectra (C-K and Ni-$L_{2,3}$ edges) corresponding to the two marked areas in the map are also depicted (thin and thick line spectra correspond to thin and thick square areas, respectively).

demonstrated to be necessary to achieve a complete chemical and structural analysis of the nanostructured ultrafine material, and has allowed the detection of heterogeneity in samples at a microscopic level. FEG and EFTEM microscopes have been very useful in providing the chemical composition of individual small nanoparticles.

It is of note that the small nanoparticles embedded in the amorphous carbon matrix are crystalline metallic nickel, formed from the reduction of Ni^{2+} (present in the as-prepared sample) by carbon during heating. A degree of surface oxidation of the nickel nanoparticles has also been detected by XAS during air exposure.

The possibility of carbon atoms sited in interstitial positions in the Ni nanocrystallite lattice could not be determined.

Acknowledgements

We thank the DGES (Project PB96-0863-C02-02) and NATO (Project CGR 97301118) for financial support. The Department of Materials (Oxford University) and the synchrotron ESRF (Dr. Michael Borowski) are acknowledged for providing the HRTEM and XAS facilities.

References

1 H. Gleiter, *Nanostruct. Mater.*, 1992, **1**, 1.
2 C. C. Koch, *Nanostruct. Mater.*, 1993, **2**, 199.
3 S. Komarneni, *J. Mater. Chem.*, 1992, **2**, 1219.
4 R. W. Siegel, *Annu. Rev. Mater. Sci.*, 1991, **21**, 559.
5 E. Matijevic, *MRS Bull.*, 1989, **XIV**, 19.
6 Y. Yoshizawa, S. Oguma and K. Yamauchi, *J. Appl. Phys.*, 1988, **64**, 6044.
7 E. F. Kneller and R. Hawig, *IEEE Trans. Magn. MAG-27*, 1991, 3588.
8 J. H. J. Scott and S. Majetich, *Phys. Rev.*, 1995, **52**, 567.
9 Y. Koltypin, A. Fernández, T. C. Rojas, J. Campora, P. Palma, R. Prozorov and A. Gedanken, *Chem. Mater.*, 1999, **11**, 1331.
10 K. S. Suslick, *Science*, 1990, **247**, 1439.
11 Yu. Koltypin, G. Kataby, X. Cao, R. Prozorov and A. Gedanken, *J. Non-Cryst. Solids*, 1996, **201**, 159.
12 J. L. Lavergne, C. Foa, P. Bongrand, D. Seux and J.-M. Martin, *J. Microsc.*, 1994, **174**, Pt 3, 195.
13 J. L. Lavergne, J.-M. Martin and M. Belin, *Microsc. Microanal. Microstruct.*, 1992, **3**, 517.
14 D. Bonin, P. Kaiser, C. Freitigny and J. Desbarres, *Stuctures Fines d'e Absorption des Rayos X en Chemie*, vol. 3, Logiciels d'Analyse, EXAFS, ed. H. Dexpert, A. Michalowizc and M. Verdagner, Societé Francaise de Chimie, Paris, 1989.
15 S. I. Zabinsky, J. J. Rehr, A. Ankudinov, R. C. Albers and M. J. Eller, *Multiple Scattering Calculations of X-Ray Absorption Spectra, Phys. Rev. B.*, 1995, **52**, 2995.
16 A. Bianconi, *X-Ray Absorption: Principles, Applications, Techniques of EXAFS, SEXAFS, and XANES*, ed. D. C. Kronigsberger and R. Prins, Wiley, New York, 1988, ch. 11, pp. 573–662.
17 T. C. Rojas, J. C. Sánchez-López, M. J. Sayagues, E. P. Reddy, A. Caballero and A. Fernández, *J. Mater. Chem.*, 1999, **9**, 1011.

Paper a908116j